



Electrophysical properties of ceramic–polymer composite films as function of sintering temperature

Sajedeh MOHAMMADI AREF¹, Mohammad GHAFOURI²

1. Faculty of Physics, University of Tabriz, Tabriz, Iran;

2. Physics Department, Shabestar Branch, Islamic Azad University, Shabestar, Iran

Received 23 January 2017; accepted 30 June 2017

Abstract: The effect of changes in sintering temperature on electrical properties and microstructure of ZnO–polyaniline–polyethylene composite ceramics, prepared in disk form at the pressure of 60 MPa and at five different temperatures, has been investigated. Increasing sintering temperature from 30 to 120 °C noticeably reduces breakdown voltage from 830 to 610 V. Further increase in sintering temperature causes breakdown voltage to increase. Interface voltage barrier height behaves differently when sintering temperature increases, which is in contrast to breakdown voltage behavior. These samples have a very low leakage current, a factor which indicates low degradation. Then again, the higher the sintering temperature gets, the less the nonlinear coefficient becomes. In addition, each sample has hysteresis which decreases through increase of sintering temperature up to 120 °C. Further increase in sintering temperature, however, causes the hysteresis loop to spread. Regarding UV spectra of the samples, it is revealed that there are three impurity levels whose behaviors against sintering temperature are subtractive. Analysis of composite samples by scanning electron microscopy indicates that their microstructure consists of grains and grain boundaries. Resistivity of grain boundaries is the main responsible factor for these changes in varistor characteristic as a function of sintering temperature.

Key words: ZnO; electrical properties; sintering temperature; varistor; composite; microstructure

1 Introduction

The need of surge protecting devices for electric power lines and electronic systems has motivated researchers to study ZnO-based electronic ceramic devices [1–3]. These devices are polycrystalline ceramics manufactured by sintering approximately 90% (molar fraction) ZnO powder, mixed with a great variety of cationic oxides such as Bi₂O₃, Sb₂O₃, MnO and CoO [4–10]. Due to their versatility, ZnO-based varistors have been widely applied in various electrical and electronic industries including power systems and semiconductor circuits in AC and DC fields, over a wide range of voltages from a few volts to tens of kilovolts, and a wide range of currents from microamperes to kilo amperes [11]. Highly nonlinear electrical behavior of ZnO varistors at high currents is quite important for applications of these devices [12–18]. It is well-known that nonlinear current–voltage characteristics of ZnO-based varistors are controlled by the well-recognized double Schottky barrier mechanism, which is triggered

by the contacting layer between ZnO grains and the second phase [19]. With the increasing demand for miniaturized devices in the electronic industry, small-sized electronic components including various low-voltage varistors are extensively desired [20]. To date, preparation methods of ZnO-based low-voltage varistors have been principally based on controlling the growth of ZnO grains or the thickness of electronic components [21–23]. In spite of their high performance, sintering temperature of these devices is still too high (more than 950 °C) [24]. Nowadays, surge arresters combine a complex metal oxide varistor technology inside a polymeric housing [25], which makes it possible to manufacture low-voltage protectors at lower sintering temperatures. While considerable research has been conducted on ceramic–polymer composite varistors, the effect of different sintering temperatures is still unavailable. Furthermore, the existing data on temperature dependence of electrical behavior of ZnO varistor ceramics are not only scarce but also contradictory. In order to study the quantitative relationship between sintering temperature and the performance

of a composite varistor, a composition of ZnO–polyaniline–polyethylene tiny particles was pressed at different sintering temperatures and its electrophysical properties were investigated.

2 Experimental

2.1 Sample preparation

Pure zinc oxide, dedoped polyaniline, and high-density polyethylene powders were sifted using a 200 U.S. mesh sieve. Then, 85% ZnO, 15% PANI and 5% HDPE (mass fraction) were weighed with the accuracy of 10^{-4} g. To have a completely homogeneous mixture, they were then admixed in a planetary mill for 8 h. Afterward, ZnO–polymer composite varistors were prepared at a pressure of 60 MPa at five different temperatures of 30, 60, 90, 120 and 130 °C. Final samples were in form of disks with a diameter of 10 mm and a thickness of 250 μ m.

2.2 Measurements of electrical properties

After observable qualities such as uniform thickness and lack of any cracks have been checked, samples were studied for their current–voltage characteristics using the two-probe method at direct current mode, after applying two copper electrodes with the effective diameter of 6 mm. By increasing the voltage to a degree which was higher than the breakdown voltage and subsequently, decreasing it to zero, it was possible to plot the hysteresis loops of the samples. UV absorption spectra of the varistors were recorded using a PHARMA spectrophotometer, SHIMADZU model 1700. UV absorption spectra, in the wavelength range of 300–1000 nm, were used to estimate the optical gap of each sample using $(ah\nu)^2$ versus $h\nu$ diagram. Finally, microstructures of samples were analyzed by investigating SEM micrographs which were obtained using MIRA3 TESCAN system.

3 Results and discussion

3.1 Current–voltage characteristics

Investigating the I – V characteristic of the prepared composite reveals that its current increases as a nonlinear function of voltage. At this type of nonlinearity, called varistor nonlinearity, I – V characteristic includes three different regions: pre-breakdown region at which the sample has high resistance, breakdown region at which resistance of the sample decreases dramatically, and upturn region at which the sample has low resistance (Fig. 1). The importance of pre-breakdown zone is due to its current, called leakage current, which is an important factor in determining sample degradation. Since current through varistor is mainly controlled by grain resistance,

an important aspect of grain resistivity in varistor ceramics is the irreversible electrical breakdown at high currents [26,27]. The nature of such electrical breakdown in varistors has not been sufficiently investigated yet. If the irreversible breakdown has a thermal nature, then it could occur due to the current instability provided that the temperature coefficient of the grain resistivity is negative [28]. It can be concluded that high leakage current results in temperature increment as a consequence of Joule heating ($Q=RI^2t$), which facilitates the development of current elements between the two electrodes. These elements let electrons flow between two conductive plates, a process which yields a perforated sample. Leakage current of this sample is very low (about 0.1 μ A), a factor which indicates low degradation. It is noteworthy that in case the applied voltage is further increased, increment of current will no longer be linear. The voltage at which nonlinear behavior starts is called breakdown voltage. At this region, the current varies as a function of voltage as follows: $I=kV^\alpha$, where k is a constant and α is the nonlinear coefficient. Greater voltage increase causes I – V characteristic to become linear again. The interesting point about this composite is that its resistance is infinite with very high accuracy (about $10^9 \Omega$) at the pre-breakdown zone, which reaches about $10^5 \Omega$ at upturn zone. In this stage, the sample could be considered an ideal voltage protector to be used in microelectronic industry.

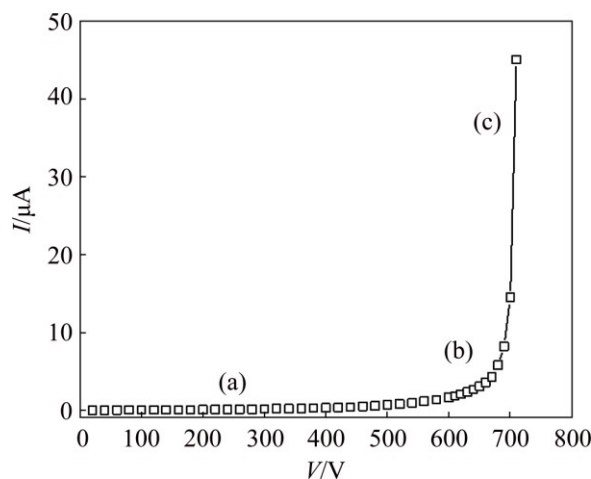


Fig. 1 I – V characteristic of composite varistor: (a) Pre-breakdown region; (b) Breakdown region; (c) Upturn region

Comparison of I – V characteristics of samples prepared at different temperatures shows that by increasing sintering temperature, breakdown voltage of samples decreases whereas their leakage current remains almost constant. Due to low leakage current (about 0.1 μ A), degradation probability is low. Breakdown voltage decrement stops once sintering temperature reaches an optimum and then, increase in sintering

temperature increases breakdown voltage while leakage current remains low (Fig. 2(a)).

3.2 Calculation of nonlinear coefficient

To calculate nonlinear coefficient, the slope of $\ln I - \ln V$ diagram at breakdown region should be calculated. This calculation reveals that increasing sintering temperature to its optimum causes nonlinear coefficient to decrease (Fig. 2(b)). Subsequently, nonlinear coefficient decreases as a result of increase in sintering temperature. It is noteworthy that compared with the corresponding GaAs–PANI–PE and Si–PANI–PE composite varistors, nonlinear coefficient is high [29,30]. This result, as well as the lower price of zinc oxide compared with gallium arsenide and silicon, makes ZnO–PANI–PE composite films a better voltage protector.

3.3 Microstructure of samples

The reason for such behaviors could be revealed by

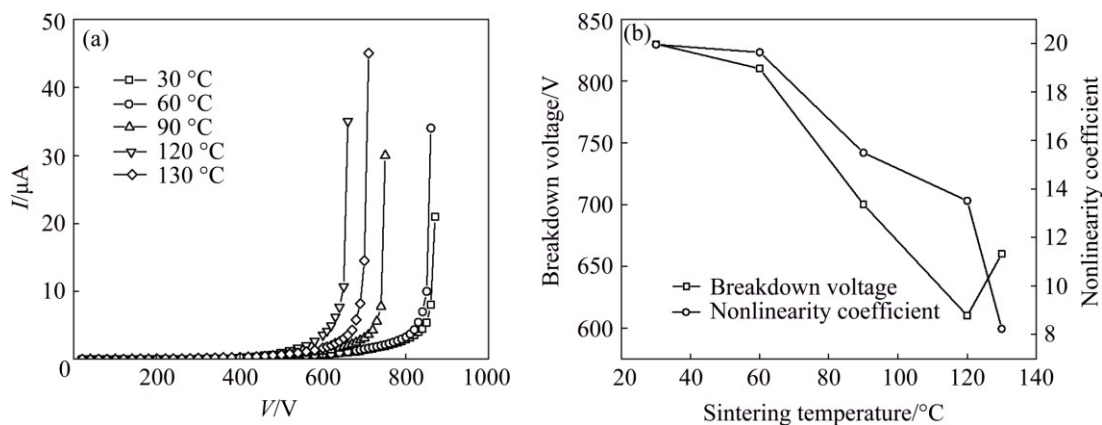


Fig. 2 I - V characteristics of samples prepared at different temperatures (a) and variation of breakdown voltage and nonlinearity coefficient versus sintering temperature (b)

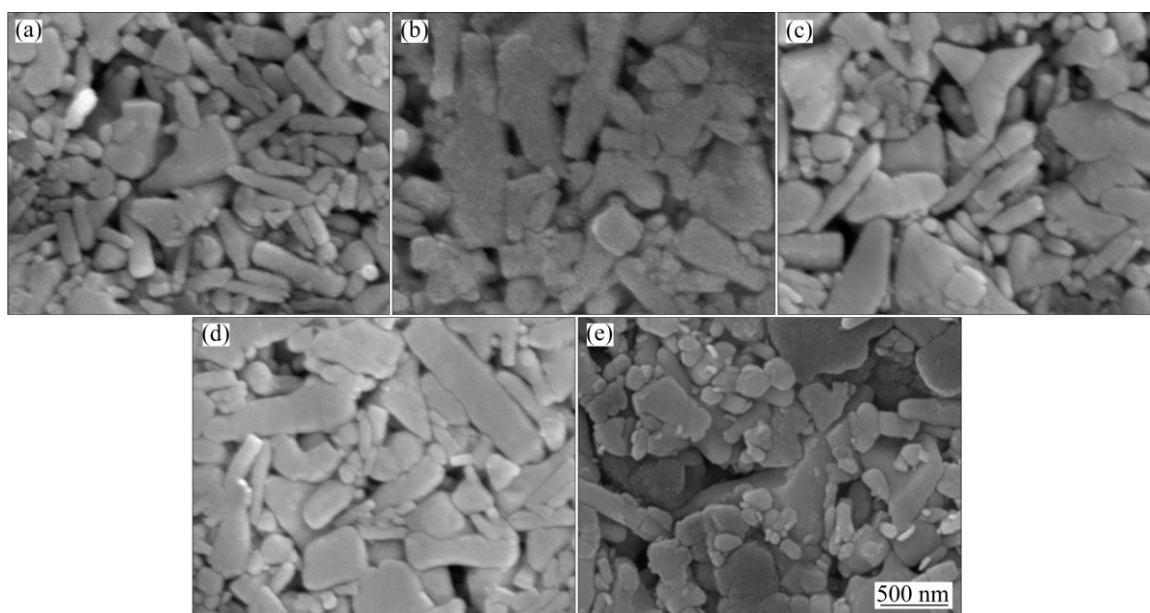


Fig. 3 SEM micrographs of samples prepared at different temperatures: (a) 30 °C; (b) 60 °C; (c) 90 °C; (d) 120 °C; (e) 130 °C

taking into consideration the SEM micrographs of the samples. Microstructure of these composites contains ZnO grains in a background of polymer matrix. These grains, as well as grain boundaries, are recognizable from Fig. 3.

It is clear that, unlike GaAs–PANI–PE composites [31], increasing sintering temperature does not clearly affect the mean size of grains. Average diameter of grains is about 240 nm. This means that in this temperature range, ZnO particles have the same opportunity to conglomerate because, compared with literature, sintering temperature of these samples is too low [24]. Therefore, the reason for such behaviors must be latent at grain boundaries. The first thing that comes to mind is that as sintering temperature approaches polyethylene melting point, PE particles become plastic. This gives PE the opportunity to admix homogeneously with PANI particles as a result of high molecular movement as well as high diffusion at high temperatures. So, inter-granular phase becomes more homogeneous, and results in low

breakdown voltage. Further increase in temperature causes PE particles to melt, which lessens the homogeneous structure of inter-granular phase once again.

3.4 Potential barrier calculation

For a more detailed discussion, it is necessary to calculate potential barriers of samples. Due to the existence of double Schottky barriers, nonlinear characteristics of ZnO-based varistors are related to grain boundaries. Schottky barrier is formed as a result of electron trapping, which is compensated by donor-like traps that exist in the depletion region of the grain boundaries [32]. Regarding this model, current density is a function of electric field as follows [33]:

$$J = AT^2 \exp[(\beta E^{1/2} - \phi_B) / kT] \tag{1}$$

where A is Richardson constant ($A = 4\rho emk^2/h^3$), ρ is the varistor density, e is the electronic charge, m is the electronic mass, k is the Boltzmann constant, h is the Planks constant, ϕ_B is the interface voltage barrier height and β is a constant. The constant β is related to the potential barrier width ($\beta \propto 1/r\omega$), where r is the number of grains per unit length and ω is the voltage barrier width. By measuring current density in the ohmic region and keeping the temperature constant, values of ϕ_B and β can be easily obtained with regard to the $(\ln J - E^{1/2})$ curve (Fig. 4). Regression calculations (least square method) clearly show that barrier height of these samples follows Eq. (1), which means that double Schottky barrier model is also applicable to ZnO–polymer composite varistors (Fig. 5). In addition to the fact that

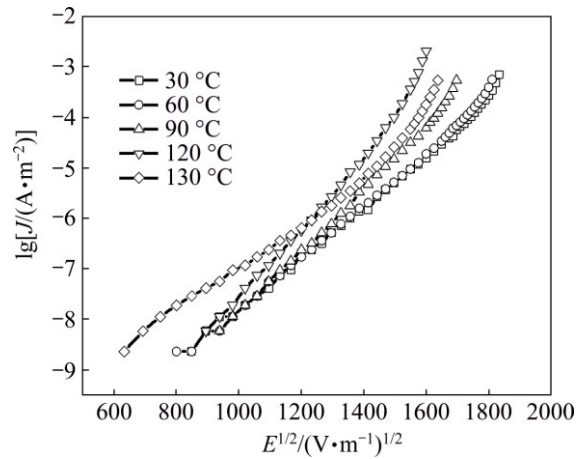


Fig. 4 $\ln J - E^{1/2}$ curves of varistor samples to calculate potential barriers

conductivity of grain boundaries of ZnO–polymer varistors is strictly contingent on PANI percentage, their inter-granular phase is made of polymer matrix instead of metal oxide additives for ZnO-based ones. The variation of ϕ_B against sintering temperature is shown in Fig. 6. It has been found out that ϕ_B increases by increasing sintering temperature to an optimum and then decreases again. Promptly, the question is why the ϕ_B behavior against sintering temperature disagrees with that of breakdown voltage. It is believed that the formation of nonlinear behavior in current types of varistors is controlled by the values of barrier voltage formed at grain boundaries compared with ϕ_B . Similar results have been reported for ZnO ceramic varistors and Fe-doped ZnO varistor [31,34,35].

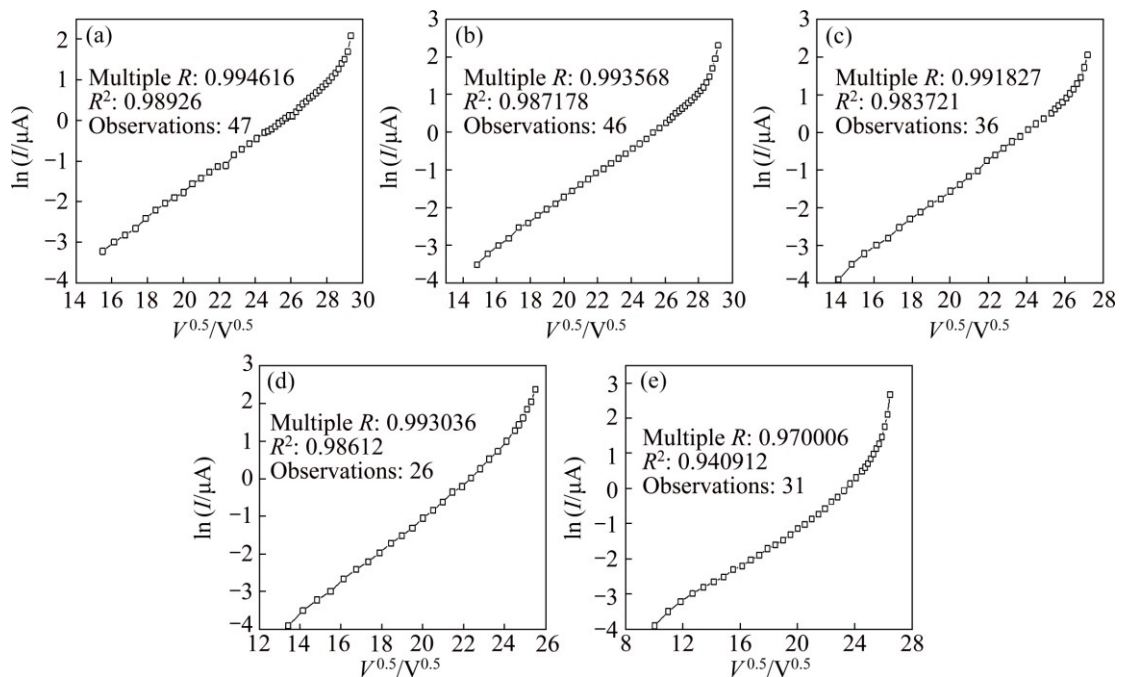


Fig. 5 Regression calculations using least square method: (a) 30 °C; (b) 60 °C; (c) 90 °C; (d) 120 °C; (e) 130 °C

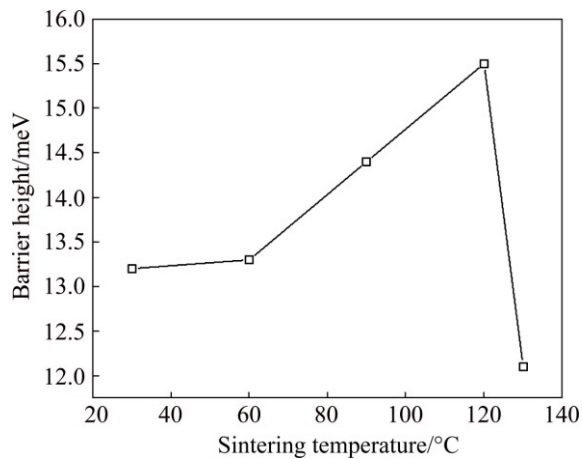


Fig. 6 Barrier height versus sintering temperature for samples

3.5 Hysteresis

Increase and subsequent decrease in applied voltage culminates in hysteresis loops that introduce 120 °C as the most prominent sintering temperature (Fig. 7). Therefore, varistor lifetime will be the longest. Hysteresis loop can be well described with regard to “dipole moments” which exist in the varistor structure. Dipole moments of atoms are randomly oriented in the absence of an external electric field. They can even be anti-parallel. By increasing the electric field, the majority of dipole moments will be oriented along the applied electric field. However, by decreasing the applied field, apparently a limited number of them could change their direction. So, most of them will remain along the externally applied electrical field. Therefore, hysteresis will be observed in the $I-V$ characteristics of varistor. As discussed earlier, when sintering temperature approaches polyethylene melting point, inter-granular phase becomes more homogeneous and, consequently, dipole moments obtain higher mobility. Greater increase in temperature lessens homogeneous structure of inter-granular phase once again.

3.6 Band gaps of samples

To calculate band gaps of the samples and

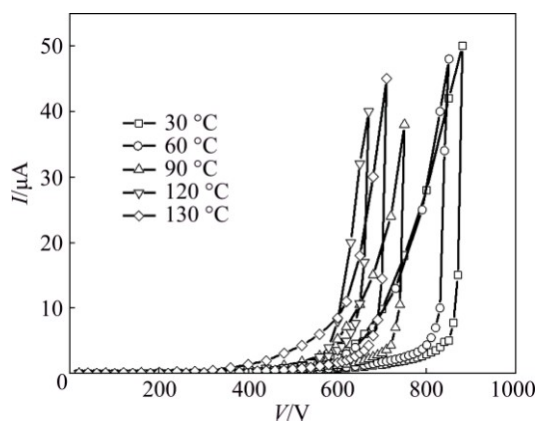


Fig. 7 Hysteresis diagrams of composite varistors

investigate the effect of sintering temperature on it, absorption spectra of the samples are helpful. By applying the Tauc model [36], the Davis and Mott model [37] in the high absorbance region, optical band gap of the samples can be calculated:

$$ahv = D(hv - E_g)^n \quad (2)$$

where hv is the incident photon energy, α is absorption, E_g is the optical band gap, and D is a constant. For a direct transition, $n=1/2$ or $2/3$; the former value is found to be more suitable for ZnO since it gives the best linear curve in the band-edge region [38,39]. By plotting the relationship between $(ahv)^2$ and hv , optical band gap of the samples is estimated; its value can then be obtained by extrapolating the linear portion of the curve to the photon energy axis in the curve. Impurity levels of the samples have a determining role on varistors. Three impurity levels are recognizable, corresponding to energies of about 0.46, 1.78 and 2 eV, respectively (Fig. 8). This means that increasing sintering temperature

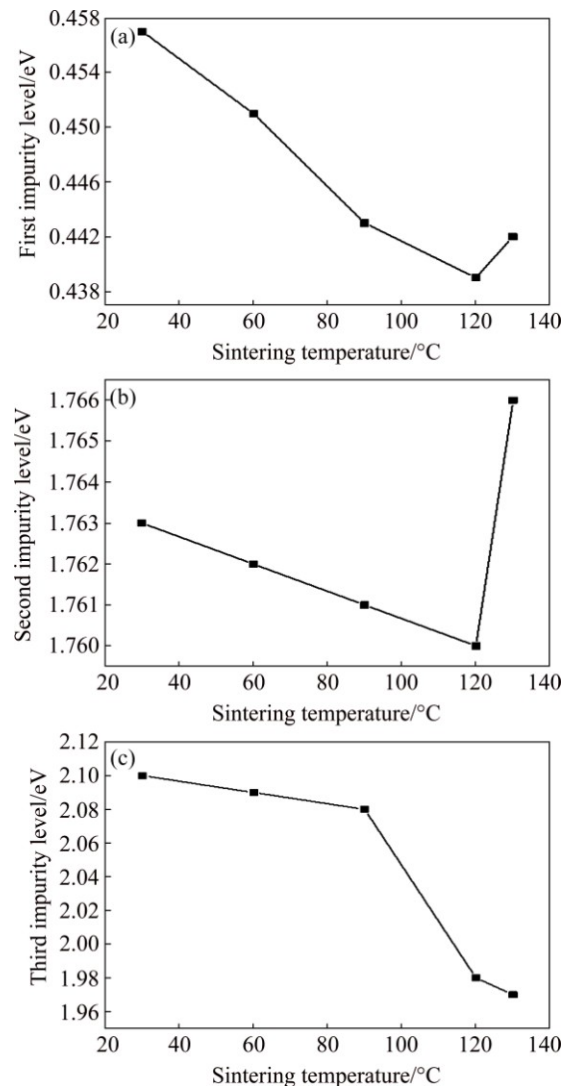


Fig. 8 Variation of three impurity levels versus sintering temperature: (a) First impurity level; (b) Second impurity level; (c) Third impurity level

does not mainly affect ΔE_g , which is the energy gap between the donor level created by the addition of polymer and the minimum of conduction band.

It is noteworthy that because of Burstein–Moss effect, optical band gap differs from electrical band gap:

$$E_O = E_g + \Delta E_{BM} \quad (3)$$

where E_O is optical band gap, E_g is electrical band gap, and ΔE_{BM} is Burstein–Moss shift. Absorption is measured at room temperature. At this temperature, the apparent band gap of a semiconductor is increased since the absorption edge is pushed to higher energies as a result of the population of all states which are close to the conduction band.

4 Conclusions

The ZnO–PANI–PE composite varistor sintered at 120 °C exhibits excellent non-ohmic properties and can, therefore, be a suitable choice for the purpose of protection from low overvoltages. Since the varistor has low degradation, its lifetime is long. As sintering temperature approaches 120 °C, breakdown voltage, nonlinearity coefficient and hysteresis decrease, but the average grain size and leakage current remain almost constant.

References

- [1] BUCHANAN R C, DEKKER M. Ceramic materials for electronics [M]. 3rd ed. New York: CRC Press, 2004.
- [2] JANOTTI A, van de WALLE C G. Fundamentals of zinc oxide as a semiconductor [J]. Reports on Progress in Physics, 2009, 72: 126–501.
- [3] FLEWITT P E J, WILD R K. Grain boundaries: Their microstructure and chemistry [M]. New York: Wiley, 2001.
- [4] BERNIK S, MACEK S, BUI A. The characteristics of ZnO–Bi₂O₃-based varistor ceramics doped with Y₂O₃ and varying amounts of Sb₂O₃ [J]. Journal of the European Ceramic Society, 2004, 24: 1195–1198.
- [5] PEITEADO M, FERNANDEZ J F, CABALLERO A C. Varistors based in the ZnO–Bi₂O₃ system: Microstructure control and properties [J]. Journal of the European Ceramic Society, 2007, 27: 3867–3872.
- [6] ABDOLLAHI Y, ZAKARIA A, AZIZ R S, TAMILI S N, MATORI K A, SHAHRANI N M, SIDEKI N M, DORRAJ M, MOOSAVI S. Optimizing Bi₂O₃ and TiO₂ to achieve the maximum non-linear electrical property of ZnO low voltage varistor [J]. Chemistry Central Journal, 2013, 7: 137–146.
- [7] HOUABES M, METZ R. Rare earth oxides effects on both the threshold voltage and energy absorption capability of ZnO varistors [J]. Ceramics International, 2007, 33: 1191–1197.
- [8] DORRAJ M, ABDOLLAHI Y, SAID S B M, SABRI MFBM, SAIRI N A, MENG W P, ABOUZARI-LOTFE E. Enhance protection of electronic appliances through multivariate modelling and optimization of ceramic core materials in varistor devices [J]. RSC Advances, 2015, 27: 21384–21395.
- [9] METZ R, DELALU H, VIGNALOU J R, ACHARD N, ELKHATIB M. Electrical properties of varistors in relation to their true bismuth composition after sintering [J]. Materials Chemistry and Physics, 2000, 63: 157–216.
- [10] DURAN P, CAPEL F, TARTAJ J, MOURE C. A strategic two-stage low temperature thermal processing leading to fully dense and fine-grained doped-ZnO varistors [J]. Advanced Materials, 2002, 14: 137–141.
- [11] FENG H, PENG Z J, FU X L, FU Z Q, WANG C B, QI L H, MIAO H Z. Effect of SnO₂ doping on microstructural and electrical properties of ZnO–Pr₆O₁₁ based varistor ceramics [J]. Journal of Alloys and Compounds, 2011, 509: 7175–7180.
- [12] GUPTA T K. Application of zinc oxide varistors [J]. Journal of the American Ceramic Society, 1990, 73: 1817–1840.
- [13] CLARKE D. Varistor ceramics [J]. Journal of the American Ceramic Society, 1999, 82: 485–502.
- [14] MARTZLOFF F D, LEVINSON L M. Surge-protective devices [C]//Electronic Ceramics: Properties, Devices and Applications 1988. New York: TMS, 1988: 275–305.
- [15] PHILIPP H R, LEVINSON L M. High-frequency and high-current studies of metal oxide varistors [J]. Journal of Applied Physics, 1976, 47: 3116–3121.
- [16] MAHMUD S, ABDULLAH M J, PUTRUS G A. Increase in upturn power dissipation of surge suppressors due to highly defective nanostructure of zinc oxide [J]. Synthesis and Reactivity in Inorganic and Metal-Organic Chemistry, 2006, 36: 3659–3664.
- [17] HU J, LONG W C, HE J L, LIU J. Influence factors of residual voltage ratio of ZnO varistor [J]. Gaodiyuan Jishu/High Voltage Engineering, 2011, 37: 554–561.
- [18] LU Z Y, QIU P, WANG X Q, CHEN Z, WU J Q, ZHANG Y P. Comparative study of microstructure and electrical properties of varistors prepared from plasma vapor-phase reaction process and french process ZnO powders [J]. Journal of the American Ceramic Society, 2011, 94: 3871–3876.
- [19] XU D, WU J T, JIAO L, XU H X, ZHANG P M, YU R H, CHENG X N. Highly nonlinear property and threshold voltage of Sc₂O₃ doped ZnO–Bi₂O₃-based varistor ceramics [J]. Journal of Rare Earths, 2013, 31: 158–163.
- [20] WANG Y, PENG Z, WANG Q, FU X. Highly nonlinear varistors from oxygen-deficient zinc oxide thin films by hot-dipping in Bi₂O₃: Influence of temperature [J]. Applied Surface Science, 2016, 390: 92–99.
- [21] PIETRZYK M A, STACHOWICZ M, JAROSZ D, MINIKAYEV R, ZIELINSKI M, DLUZEWSKI P, KOZANECKI A. Properties of ZnO/ZnMgO nanostructures grown on r-plane Al₂O₃ substrates by molecular beam epitaxy [J]. Journal of Alloys and Compounds, 2015, 650: 256–261.
- [22] YOON Y C, PARK K S, KIM S D. Effects of low preheating temperature for ZnO seed layer deposited by sol–gel spin coating on the structural properties of hydrothermal ZnO nanorods [J]. Thin Solid Films, 2015, 597: 125–130.
- [23] IVON A I, GLOT A B, LAVROV R I, BUBEL T A. Temperature dependence of zinc oxide grain resistivity in ZnO varistor ceramics [J]. Journal of Alloys and Compounds, 2016, 656: 740–744.
- [24] XIAO X, ZHENG L, CHENG L, TIAN T, RUAN X, LI G. Effect of Cr₂O₃ on the property and microstructure of ZnO–Bi₂O₃ varistor ceramics in different sintering temperature [J]. Ceramics International, 2015, 41(S): s557–s562.
- [25] de SALLES C, NOGUEIRA T A, NETO E T W, MARTINEZ M L B, de QUEIROZ A A A. Effects of operation temperature in artificially aging of zinc oxide varistors by high current short impulses [J]. Electric Power Systems Research, 2016, 134: 145–151.
- [26] EDA K. Destruction mechanism of ZnO varistors due to high currents [J]. Journal of Applied Physics, 1984, 56: 2948–2955.
- [27] VOJTA O A, CLARKE D R. Microstructure of current localization and “puncture” failure in varistor ceramics [J]. Journal of Applied

- Physics, 1997, 81: 985–993.
- [28] HUNG N T, QUANG N D, BERNIK S. Electrical and microstructural characteristics of ZnO–Bi₂O₃-based varistors doped with rare-earth oxides [J]. *International Journal of Materials Research*, 2001, 16: 2817–2823.
- [29] BIDADI H, MOHAMMADI AREF S, GHAFOURI M, PARHIZKAR M. Effect of changing Gallium arsenide content on Gallium arsenide–polymer composite varistors [J]. *Journal of Physics and Chemistry of Solids*, 2013, 74: 1169–1173.
- [30] GHAFOURI M, PARHIZKAR M, BIDADI H, MOHAMMADI AREF S, OLAD A. Effect of Si content on electrophysical properties of Si-polymer composite varistors [J]. *Materials Chemistry and Physics*, 2014, 147: 1117–1122.
- [31] BIDADI H, MOHAMMADI AREF S, GHAFOURI M, PARHIZKAR M, OLAD A. The effect of sintering temperature on varistor characteristics of gallium arsenide–polyaniline–polyethylene composite varistors [J]. *Materials Science in Semiconductor Processing*, 2013, 16: 752–758.
- [32] WILLIAMS P, KRIVANEK O, THOMAS G, YODOGAWA M. Microstructure-property relationships of rare-earth–zinc-oxide varistors [J]. *Journal of Applied Physics*, 1980, 51: 3930–3934.
- [33] PIANARO S, BUENO P, OLIVI P, LONGO E, VARELA J. Effect of Bi₂O₃ addition on the microstructure and electrical properties of the SnO₂–CoO–Nb₂O₅ varistor system [J]. *Journal of Materials Science Letters*, 1997, 16: 634–638.
- [34] SEDKY A, ABU-ABDEEN M, ALMULHEM A A. Nonlinear *I-V* characteristics in doped ZnO based-ceramic varistor [J]. *Physica B*, 2007, 388: 266–273.
- [35] HAN J, SENOS A M R, MANTAS P Q. Deep donors in polycrystalline Mn-doped ZnO [J]. *Materials Chemistry and Physics*, 2002, 75: 117–120.
- [36] TAUC J. *Amorphous and liquid semiconductors* [M]. London: Plenum, 1974.
- [37] DAVIS E A, MOTT N F. *Conduction in non-crystalline systems V. Conductivity, optical absorption and photoconductivity in amorphous semiconductors* [J]. *Philosophical Magazine*, 1970, 22: 903–922.
- [38] TAN S T, SUN X W, ZHANG X H, CHEN B J, CHUA S J, YONG A, DONG Z L, HU X. Zinc oxide quantum dots embedded films by metal organic chemical vapor deposition [J]. *Journal of Crystal Growth*, 2005, 290: 518–522.
- [39] LU J G, YE Z Z, WANG L, HUANG J Y, ZHAO B H. Structural, electrical and optical properties of N-doped ZnO films synthesized by SS-CVD [J]. *Materials Science in Semiconductor Processing*, 2002, 5: 491–496.

陶瓷–高分子复合薄膜的电物理性能随烧结温度的变化

Sajedeh MOHAMMADI AREF¹, Mohammad GHAFOURI²

1. Faculty of Physics, University of Tabriz, Tabriz, Iran;

2. Physics Department, Shabestar Branch, Islamic Azad University, Shabestar, Iran

摘要: 在 60 MPa 压力, 5 个不同的烧结温度下将 ZnO–聚苯胺–聚乙烯混合粉末压制成复合陶瓷圆片, 研究烧结温度的变化对其电物理性能和显微组织的影响。结果显示, 烧结温度从 30 °C 升高至 120 °C, 击穿电压从 830 V 降低至 610 V; 继续提高烧结温度, 击穿电压反而升高。随着烧结温度的升高, 界面电压势垒的变化与击穿电压的变化相反。样品的泄露电流很低, 说明材料具有低的降解速率。烧结温度越高, 非线性系数变得越小。此外, 各样品均有迟滞现象, 随烧结温度升高至 120 °C, 电滞回线降低; 当温度继续升高时, 电滞回线变宽。紫外光谱的结果显示, 有 3 个杂质能级, 且随烧结温度的升高而降低。扫描电镜的结果显示, 复合材料显微组织中含有晶粒和晶界, 晶界的电阻率是影响材料的压敏特性随烧结温度变化的主要因素。

关键词: ZnO; 电性能; 烧结温度; 压敏电阻; 复合材料; 显微组织

(Edited by Bing YANG)